Citation: Abdellah Benchekkour, Nazihe Terfaya, Mohammed Elmir, et al. Thermal and friction effects on mixed mode delamination. *Journal of Harbin Institute of Technology(New Series)*. DOI:10.11916/j.issn.1005-9113.2024034.

Thermal and Friction Effects on Mixed Mode Delamination

Abdellah Benchekkour[1], Nazihe Terfaya[2], Mohammed Elmir[3] and Barhm Abdullah Mohamad[4]*

(*1. ENERGARID Laboratory, Tahri Mohammed University, Bechar 08000, Algeria;*
2. FIMAS Laboratory, Tahri Mohammed University, Bechar 08000, Algeria;
3. L2ME Laboratory, Tahri Mohammed University, Bechar 08000, Algeria;
4. Department of Petroleum Technology, Koya Technical Institute, Erbil Polytechnic University, Erbil 44001, Iraq)

Abstract: A comprehensive numerical investigation into mixed-mode delamination is presented in this study. It aims to assess the impact of thermal and friction effects through mixed-mode flexure crack propagation testing. Finite element analysis was employed to model the delamination process, incorporating a contact cohesive zone model. This model couples the traction-separation law, the contact law, and the Coulomb friction law simultaneously. The thermomechanical analysis in this study is performed using a sequentially coupled approach, implemented with the finite element software ABAQUS. The findings underscore the importance of this study.

Keywords: delamination; mixed mode; thermal effect; friction effect; contact cohesive model

CLC number: TB303 **Document code**: A **Article ID**: 1005-9113(2024)00-0000-08

0 Introduction

The delamination phenomenon is a common occurrence in structures and materials, often arising from mode I, mode II, or a combination of both modes, known as mixed-mode delamination. In practical scenarios, structures typically experience a combination of these modes. The combined action of forces on structures can lead to the formation of small cracks at the interface, while pre-existing cracks may also propagate under these operational forces. Understanding crack formation and propagation is crucial in fracture mechanics studies [1-2]. For this purpose, various specimens have been proposed in the literature to study mixed-mode delamination, but many of them have practical limitations that limit their widespread use. In these tests, a crack is initially introduced between two materials and propagates under a bending load [3]. Among these tests, mixed-mode flexure (MMF) stands out, utilizing a combination of pure propagation modes (traction and shear), which reliably simulate the structures behavior[4].

Modeling delamination under mixed-mode conditions remains an active research area, with new approaches including phase-field modeling[5], analytical modeling[6], fatigue delamination[7], and experimental investigation[8]. Additionally, to tackle the complexities of delamination in structures, researchers have developed advanced techniques based on the finite element method. Cohesive Zone Modeling (CZM) has emerged as a prominent approach for simulating the nonlinear behavior of interfaces during delamination. It offers a more comprehensive understanding of delamination behavior, considering various physical phenomena such as thermal effects and friction at the interface between delaminated layers[9].

In this context, numerous studies have been undertaken on the thermal effects on this mode. Ribas et al.[10] investigated the influence of temperature on mixed-mode fatigue crack propagation. Kim et al. [11] analyzed the impact of temperature on the interfacial adhesion of electronic components using a four-point bending test. In addition, Li et al. [12] studied the thermomechanical delamination mechanisms in segmented multilayered high-temperature coating

Received 2024-04-04.

Corresponding author. Abdellah Benchekkour, PhD. Email: benchekkour.abdellah@univ-bechar.dz

systems. Zhang et al.[13] investigated fatigue crack propagation in the slab track interface under cyclic temperature loads. Zhang et al.[14] examined the temperature effect on the fracture energy of adhesive layers. On the other hand, most studies have used the cohesive element technique for delamination simulation; however, this technique neglects interface phenomena such as friction. To achieve more realistic predictions, the contact cohesive technique considers these interfacial problems. In this context, recently, Benchekkour et al.[15] studied the thermal effect on the delamination process between an elastic body and a rigid support in modes I and II, considering the friction effect. The present study, unprecedented in its scope, contributes novel insights by examining the combined influence of thermal effects and delaminated surface phenomena such as friction on mixed-mode delamination behavior. A contact cohesive model that couples unilateral contact and the Coulomb law of friction is employed. For the thermal effect, a sequential thermomechanical coupling is utilized. Different thermal boundary conditions and friction coefficients are used to study the delamination process in mixed-mode flexure test.

1 Mathematical Model and Numerical Method

In the present study, a multi-physics approach is adopted, where two distinct aspects are addressed. Firstly, the fracture behavior of solids and the interactions at their interfaces are simulated using a contact cohesive zone model. This model enables the analysis of crack initiation and propagation. Secondly, a thermal problem is considered to account for temperature-dependent effects on the delamination behavior. The coupling between these two problems occurs sequentially.

1.1 Contact Cohesive Zone Model

The complexity of the mixed mode delamination requires the use of the contact cohesive zone model. The current model based on two fundamental aspects: the contact mechanics and fracture mechanics. Firstly, for contact approach, the frictional unilateral contact problem is used. These problems are characterized by a non-regular boundary condition and can be formulated with evolutionary variational inequations or differential inclusions. The unilateral contact conditions allow for separation and no penetration between two bodies in contact. These conditions are also known as the Signorini conditions[16], are expressed as follows:

$$\dot{u}_n \geqslant 0, R_n \geqslant 0, R_n \dot{u}_n = 0 \tag{1}$$

where R_n, $\dot{u}_n$ represent the contact force and the normal relative velocity respectively. In addition, when the frictional threshold is directly proportional to the normal contact force, the problem corresponds to the Coulomb friction problem, and is typically expressed as:

$$\begin{cases} \|R_t\| \leqslant \mu \cdot R_n, if\ u_t = 0 \\ \|R_t\| = -\mu \cdot R_n \dfrac{\dot{u}_t}{\|\dot{u}_t\|}, \text{if } \dot{u}_t \neq 0 \end{cases} \tag{2}$$

where R_t is the friction force; μ is the friction coefficient; u_t is the sliding; and $\dot{u}_t$ is the sliding velocity. In this context, the interface behavior takes three possibilities: no contact, sticking, or sliding, as the unilateral contact and Coulomb friction law are combined to form a well posed problem.

In fracture modeling, numerous techniques have been developed. CZM is particularly useful for simulating damage initiation and propagation. Additionally, CZM can be easily coupled with more complex problems[9]. Furthermore, it describes the relationship between stresses and relative displacements, as shown in the pioneer works[17-18]. In more detail, the delamination behavior is divided into three stages. Firstly, the elastic behavior is simulated up to a certain threshold $\sigma_{\max}^{\mathrm{Coh}}$. Then, subsequent softening models the degradation of material properties up to failure, followed by addressing frictional contact behavior in the final stage. This behavior is also known as the traction separation law. Damage initiation can be determined using various criteria. This study focuses on employing the quadratic nominal stress criterion to define the onset of damage[19], as follows:

$$\max\left[\frac{\langle \sigma_{\mathrm{n}}^{\mathrm{Coh}} \rangle}{\sigma_{\mathrm{n}}^{\mathrm{Coh}0}}, \frac{\sigma_{\mathrm{t}}^{\mathrm{Coh}}}{\sigma_{\mathrm{t}}^{\mathrm{Coh}0}}\right] = 1 \tag{3}$$

where $\sigma_{\mathrm{n}}^{\mathrm{Coh}0}$ and $\sigma_{\mathrm{t}}^{\mathrm{Coh}0}$ denote the peak values of the nominal stress when the deformation is purely normal to the interface or purely in the first or second shear direction, respectively. In addition, σ^{Coh} is the vector of nominal traction, with $\sigma_{\mathrm{n}}^{\mathrm{Coh}}$ and $\sigma_{\mathrm{t}}^{\mathrm{Coh}}$ representing the nominal tractions in the normal and tangential directions, respectively. The elastic behavior is descibed as follows[19]:

$$\boldsymbol{\sigma}^{\mathrm{Coh}} = \begin{Bmatrix} \sigma_{\mathrm{n}}^{\mathrm{Coh}} \\ \sigma_{\mathrm{t}}^{\mathrm{Coh}} \end{Bmatrix} = \begin{bmatrix} K_{\mathrm{nn}} & K_{\mathrm{nt}} \\ K_{\mathrm{nt}} & K_{\mathrm{tt}} \end{bmatrix} \begin{bmatrix} \delta_{\mathrm{n}} \\ \delta_{\mathrm{t}} \end{bmatrix} = K\delta \tag{4}$$

where K_{nn} and K_{tt} represent the normal and tangential contact stiffness, respectively, while δ_n and δ_t denote the normal and tangential separations, respectively.

The damage evolution is described as shown in Eq.(5), representing the degradation by a scalar damage term D:

$$\sigma^{\mathrm{Coh}} = (1 - D)\sigma^{\overline{\mathrm{Coh}}} \tag{5}$$

where $\sigma^{\overline{\mathrm{Coh}}}$ denotes the stress tensor computed in the current increment without considering damage. Moreover, complete separation is typically anticipated by a linear power law expression of the necessary energies for failure in the pure modes, as shown in Eq.(6), where the power law exponent is $\alpha = 1$.

$$\left\{\frac{G_n}{G_n^c}\right\}^{\alpha} + \left\{\frac{G_t}{G_t^c}\right\}^{\alpha} = 1 \tag{6}$$

where G_n represent the work performed by tractions and their corresponding relative displacements in the normal direction, while G_t represents the work done in the shear direction. Similarly, G_n^c and G_t^c denote the critical fracture energies needed to induce failure in the normal and shear directions, respectively.

1.2 Contact Cohesive Thermal Analysis

To analyze coupled problems, several approaches are used. In the present study, the problem is solved sequentially, where the stress/displacement solution relies on a temperature field without any reverse dependencies. In such contexts, equations are tackled in sequence. Initially, the thermal analysis is conducted to determine the temperature distribution. Specifically, the heat conduction equation, under steady-state conditions, is employed for this purpose:

$$\frac{\partial^2 T}{\partial x^2} + \frac{\partial^2 T}{\partial y^2} = 0 \tag{7}$$

The temperature distribution allows for the determination of the thermal relative displacement component ε_{th}. It is determined by incorporating the temperature change ΔT and the coefficient of thermal expansion α, as follows:

$$\varepsilon_{th} = \alpha \Delta T \tag{8}$$

The global relative displacement ε, considering thermal effects, is expressed as:

$$\varepsilon = \varepsilon_{mec} + \varepsilon_{th} \tag{9}$$

Then, in the cohesive contact analysis, the cohesive model describes the behavior of the interface prior to and during the onset of failure. Once cohesive failure occurs, the interface can no longer sustain any tensile or shear stress, and the contact model then governs the subsequent interaction between the surfaces. The coupled cohesive contact is represented by the sum of contact force R^{cont} and cohesive force R^{Coh}, as illustrated:

$$R^{\mathrm{total}} = R^{\mathrm{cont}} + R^{\mathrm{Coh}} \tag{10}$$

The mixed behavior can be delineated into normal and tangential behavior. For the normal behavior, coupled cohesive unilateral conditions are as follows:

$$R_n^{\mathrm{total}} = R_n^{\mathrm{cont}} + R_n^{\mathrm{Coh}} \tag{11}$$

Similarly, the tangential behavior is expressed by a coupled cohesive Coulomb friction law:

$$R_t^{\mathrm{total}} = R_t^{\mathrm{cont}} + R_t^{\mathrm{Coh}} \tag{12}$$

Furthermore, the finite element formulation for resolving the mixed mode, considering both thermal and friction effects, is derived:

$$[\boldsymbol{K}_g][\boldsymbol{U}] = [\boldsymbol{F}_g] + [\boldsymbol{R}^{\mathrm{cont}}] + [\boldsymbol{R}^{\mathrm{Coh}}] + [\boldsymbol{F}_{\mathrm{thg}}] \tag{13}$$

where $[\boldsymbol{K}_g]$ is the stiffness matrix, $\{\boldsymbol{U}\}$ is the displacement vector, $[\boldsymbol{F}_g]$ is the global force vector, and $[\boldsymbol{F}_{\mathrm{thg}}]$ is the global thermal force vector.

2 Problem Description

This study focuses on a mixed-mode flexure crack propagation test, integrating thermal and friction effects. The analysis utilizes a contact cohesive model implemented within the standard finite element software ABAQUS. A steady-state thermal analysis is conducted, employing a node-to-surface technique for contact interaction. To solve coupled problems, a Lagrange multiplier method is employed, and the resolution scheme is sequential used. Fig. 1 shows the geometry with the boundary conditions of MMF test[20]. This example involves utilizing a two-layer beam previously cracked at its interface. The methodology includes conducting a three-point flexure test. Initially, the two layers of the beam are adhered together, and it is subjected to a vertical load of F = 1 N over a duration of 1 s.

The linear elastic model is employed, with the material characterized by a Young's modulus of 70000 MPa and a Poisson's ratio of $\nu = 0.3$. Additionally, the thermal properties include a thermal conductivity of $\lambda = 230$ W/(m·K) and a thermal expansion coefficient of $\alpha_{th} = 23 \times 10^{-6}$/K. Also, the cohesive parameters required for the analysis are: the decohesion energy is 10^{-5} mJ/mm^2, the maximal cohesive stress (for normal and tangential directions) is 0.00283 MPa, the initial stiffness of the interface is 10^4 MPa/mm, and the friction coefficient is 0.2.

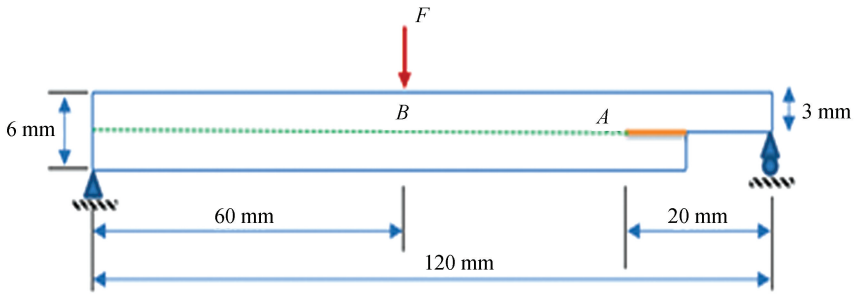

Fig.1 Geometry and boundary conditions of MMF test

The mesh was defined using a linear quadrilateral element (CPE4R), while the interface was discretized using 110 nodes. The calculation process was carried out over 1000 steps, allowing a detailed temporal analysis of the cracking behavior. Deformed meshes were generated at three specific time instants, namely t_1, t_2, and t_3, as shown in Fig. 2.

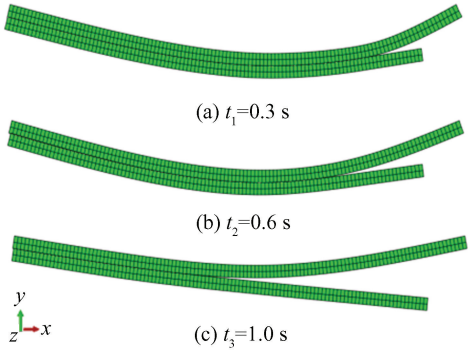

Fig. 2 The deformed meshes

3 Results and Discussion

3.1 Thermal Effect

In this section, the influence of the presence of thermal field in mixed mode delamination is studied, through a mixed mode flexure test. The thermal boundary conditions closely mirror those outlined in Ref.[15], with four states of imposed temperature on the upper face of the upper structure (T_{sup} = 25, 50, 75, and 100 ℃) and a constant temperature (T_{right} = 50 ℃) on the right lateral edge of the upper structure.

Fig. 3 shows the evolution of the distribution of normal and tangential stresses (σ_n^{tot}, σ_t^{tot}) along the interface for three-time steps, with and without thermal effects. In the latter case, we take into account a temperature of T_{sup} = 100 ℃. It can be observed from these figures that there is a significant generation of tangential stresses at the onset of cracking due to the presence of the thermal field. Then, during the second step, as crack propagation occurs, there is a concentration of tangential and normal stresses, particularly in the region where the force is applied, leading to cracking followed by a reduction in normal stresses due to separation. In the latter stages, a regeneration of tangential and normal stresses in the adherent part is observed due to thermal stresses. It is easy to notice the thermal influence on the mixed mode, especially in the tangential behavior.

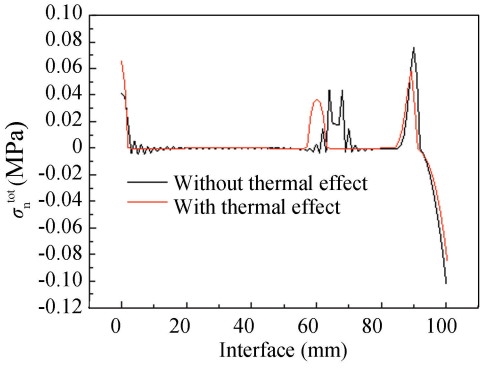

(a) Normal stress distribution along the interface for t = 0.3 s

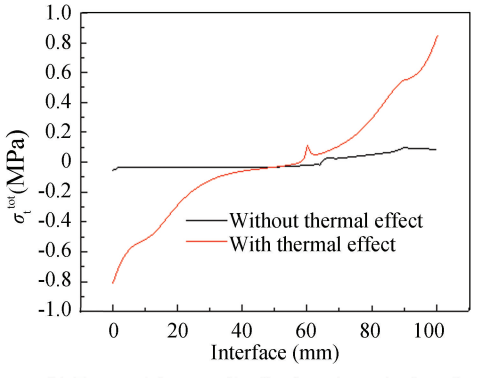

(b) Tangential stress distribution along the interface for t = 0.3 s

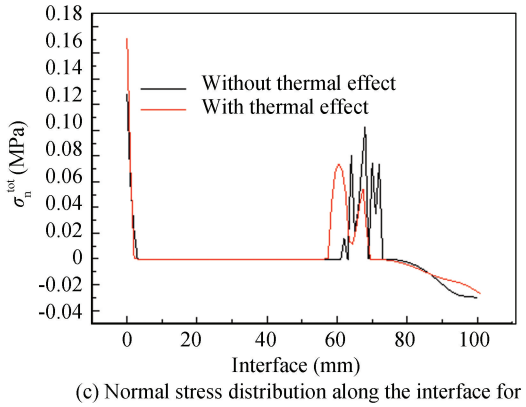

(c) Normal stress distribution along the interface for $t = 0.6$ s

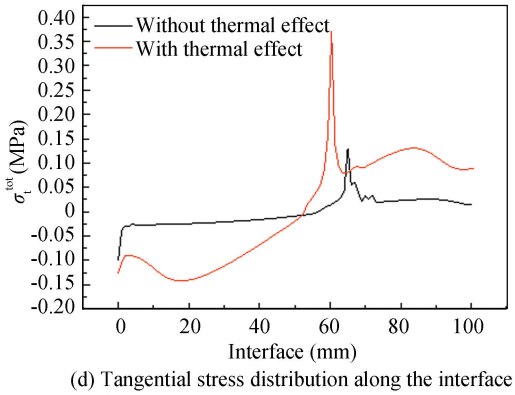

(d) Tangential stress distribution along the interface for $t = 0.6$ s

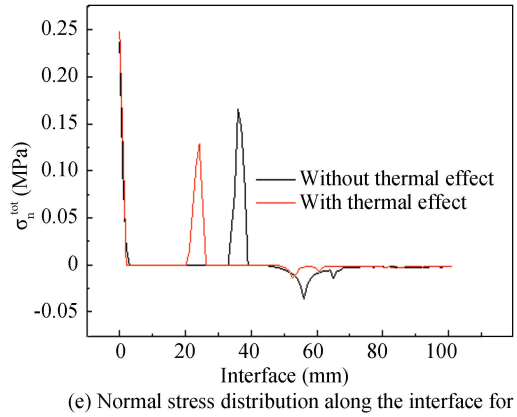

(e) Normal stress distribution along the interface for t=1.0 s

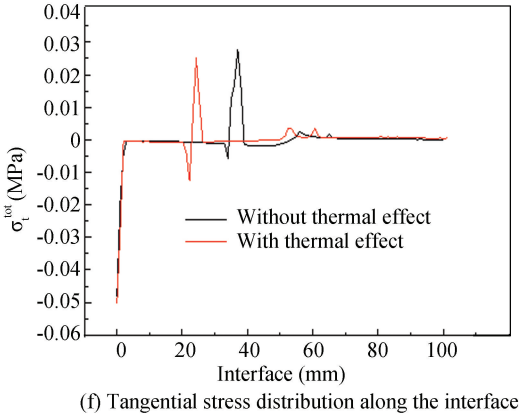

(f) Tangential stress distribution along the interface for $t = 1.0$ s

Fig. 3 Evolution of the distribution of normal and tangential stresses along the interface for three-time steps

As observed in the previous paragraph, the behavior is affected at two main points (as shown in Fig. 1): Point A, corresponding to the delamination initiation, and point B, marking the concentration of the force. To better understand mixed-mode delamination, the behavior at these two points is investigated. Fig. 4 illustrates how the normal and tangential stresses evolve as a function of debonding (u_n) and sliding (u_t), respectively, at points A and B, with and without considering the thermal effect.

In the context of normal behavior, it is essential to note that the thermal effect induces an acceleration of delamination initiation at point A. Furthermore, when the thermal gradient is higher, the separation is rapid, caused by the elastic energy becoming larger than the limit of decohesion energy, which poses a Signorini problem. However, at point B, in the middle of the interface, the thermal effect is negligible on the delamination behavior, except in the case where the temperatures are identical, which can cause a delay in the separation.

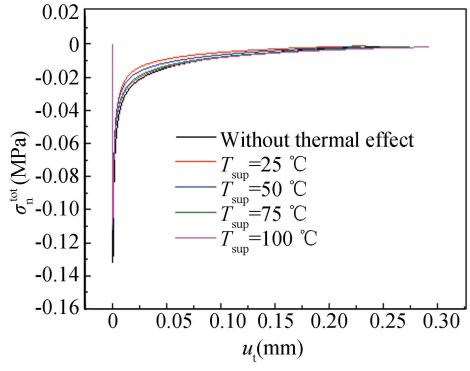

(a) Evolution of normal stress as a function of separation for point A

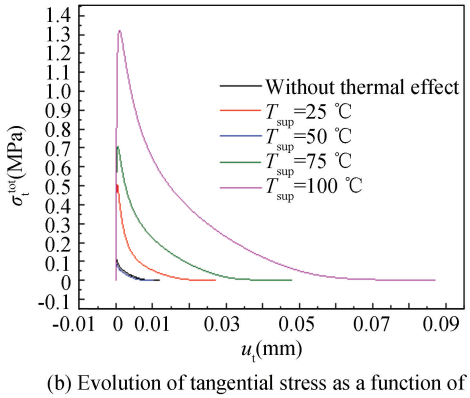

(b) Evolution of tangential stress as a function of sliding for point A

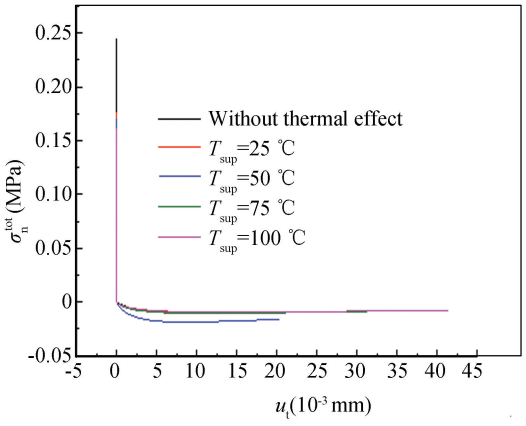

(c) Evolution of normal stress as a function of separation for point *B*

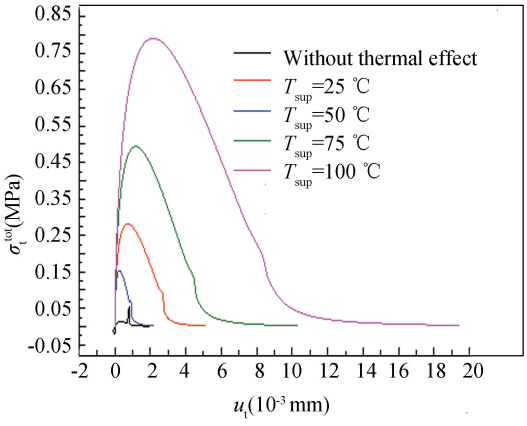

(d) Evolution of tangential stress as a function of sliding for point *B*

Fig. 4 Evolution of normal and tangential stresses as a function of separation and sliding, respectively, at points *A* and *B*

On the other hand, the tangential behavior is more influenced by the presence of a thermal field. By analyzing the various thermal boundary conditions, it can easily be seen that the increase in the thermal gradient generates greater cohesive stresses, leading to a delay in the delamination initiation. Furthermore, by comparing the behaviors between points *A* and *B*, it can be observed that there is an accelerated initiation at point *B* compared to *A*, due to the concentration of forces at this point. Thus, a brittle fracture at point *A* in relation to *B* is noticed, because point *A* represents the crack tip.

In addition, in all cases, the elastic behavior is similar, except at the initiation and evolution of damage, and also in the complete failure, where the classic friction problem is observed. In the latter case, when the gradient is higher, the separation is faster. Therefore, the following paragraph delves into the influence of friction on mixed-mode delamination behavior.

3.2 Friction Effect

The evolution of sliding at point *A* as a function of the friction coefficient is depicted in Fig. 5, both without and with the inclusion of thermal effects. In the thermal case, T_{sup} = 100 ℃ is taken. Notably, the influence of friction at point *A* appears negligible in both scenarios, without and with thermal effects, as this point serves as a critical location, specifically the crack tip. However, there is a notable importance of friction effect in the middle of the interface. Furthermore, the impact of the thermal field remains significant. These findings underscore the necessity of considering thermal effects in delamination analysis.

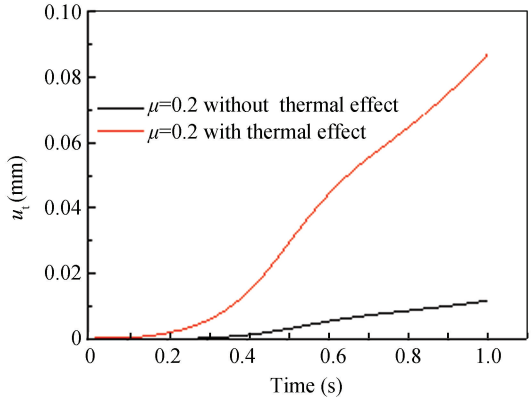

(a) Evolution of sliding at a coefficient of friction equal to 0.2

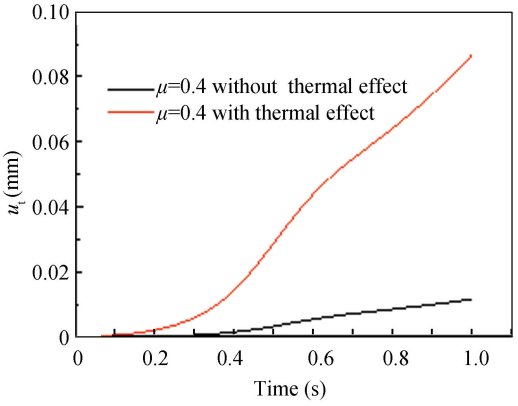

(b) Evolution of sliding at a coefficient of friction equal to 0.4

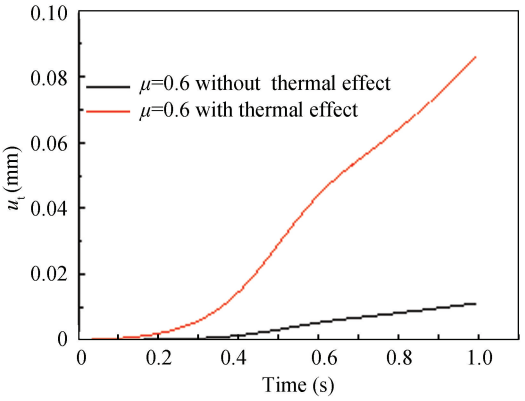

(c) Evolution of sliding at a coefficient of friction equal to 0.6

Fig.5 Evolution of sliding as a function of the coefficient of friction

4 Conclusions

The comprehensive investigation conducted in this study on mixed-mode delamination, considering both thermal and friction effects through a contact cohesive zone model in ABAQUS, underscores several key insights. Firstly, it highlights the substantial impact of thermal effects on delamination behavior, particularly evident in damage initiation and evolution stages. Moreover, the analysis reveals that in mixed-mode directions, the tangential behavior experiences a more pronounced influence from thermal effects compared to the normal behavior. Additionally, the significance of friction on the delaminated surface is observed to be notable in the interface middle but deemed negligible near the crack tip.

References

[1] Peng G, Yang J. Residual mechanical properties and explosive spalling behavior of ultra-high-strength concrete exposed to high temperature. Journal of Harbin Institute of Technology (New Series), 2017,24(4): 62-70.DOI:10.11916/j.issn.1005-9113.16096.

[2] Zahri N A M, Yusof F, Miyashita Y, et al. Effect of porous copper pore density on joint interface: microstructure and mechanical analysis. Journal of Harbin Institute of Technology (New Series), 2022,29(1):24-31. DOI: 10.11916/j.issn.1005-9113.2020056.

[3] Benzeggagh M L, Kenane M Measurement of mixed-mode delamination fracture toughness of unidirectional glass/epoxy composites with mixed-mode bending apparatus. Composites Science and Technology, 1996,56(4):439-449.DOI:10.1016/0266-3538(96)00005-X.

[4] Bae H, Kang M, Woo K, et al. Test and analysis of modes I, II and mixed-mode I/II delamination for carbon/epoxy composite laminates. International Journal of Aeronautical and Space Sciences, 2019,20:636-652.DOI: 10.1007/s42405-019-00170-9.

[5] Mrunmayee S, Rajagopal A, Rakesh K, et al. Phase field approach to predict mixed-mode delamination and delamination migration in composites. Composite Structures, 2024,337:118074.DOI:10.1016/j.compstruct.2024.118074.

[6] Kotsinis G, Loutas T. An analytical solution of the total strain energy release rate and mode partitioning of a beam type delamination specimen under high speed mixed-mode loading. Engineering Fracture Mechanics, 2023, 279: 109018.DOI:10.1016/j.engfracmech.2022.109018.

[7] Ahmad S, Khan R, Amjad M, et al. Fatigue delamination behavior of GFRP composites under mixed-mode I/II loading. Iranian Journal of Chemistry and Chemical Engineering, 2023,42(10):3546-3554.

[8] Chen Y, Liu K, Xu Z, et al. A comprehensive experimental investigation of the rate-dependent interlaminar delamination behaviour of CFRP composites. Composites Part B: Engineering, 2023,261:110788.DOI: 10.1016/j.compositesb.2023.110788.

[9] Elices M, Guinea G V, Gomez J, et al. The cohesive zone model: advantages, limitations and challenges. Engineering Fracture Mechanics, 2002,69(2):137-163. DOI:10.1016/S0013-7944(01)00083-2.

[10] Ribas M, Akhavan-Safar A, Carbas R J C, et al. Mixed mode fatigue crack growth and fatigue threshold analysis in polyurethane adhesives at elevated temperatures. International Journal of Fatigue, 2024,183:108275.DOI: 10.1016/j.ijfatigue.2024.108275.

[11] Kim G, Son K, Kim Y C, et al. Effects of dielectric curing temperature on the interfacial reliability of Cu/Ti/PBO for FOWLP applications. Electronic Materials Letters, 2024,20:393-401.

[12] Li B, Yang B, Wang S, et al. Numerical study of thermomechanical delamination mechanisms in segmented high-temperature coatings. Engineering Failure Analysis, 2023, 153: 107577. DOI: 10. 1016/j. engfailanal. 2023. 107577.

[13] Zhang J, Zhu S, Cai, C. et al. Cohesive zone modeling of fatigue crack propagation in slab track interface under cyclic temperature load. Engineering Failure Analysis, 2022, 134: 106028. DOI: 10. 1016/j. engfailanal. 2022. 106028.

[14] Zhang Z, Dasari A. Effect of temperature on the fracture energy of adhesive layers of engineered wood. International Journal of Adhesion and Adhesives, 2022, 117 (Part A): 103185. DOI: 10. 1016/j. ijadhadh. 2022. 103185.

[15] Benchekkour A, Terfaya N, Elmir M, et al. Modeling of delamination process coupling contact, friction, and adhesion considering the thermal effect. Materials Physics and Mechanics, 2023, 51(3): 146-166. DOI: 10.18149/MPM.5132023_15.

[16] Raous M, Cangémi L, Cocu M. A consistent model coupling adhesion, friction, and unilateral contact. Computer Methods in Applied Mechanics and Engineering, 1999, 177(3-4): 383-399. DOI: 10.1016/S0045-7825(98)00389-2.

[17] Dugdale D S. Yielding of steel sheets containing slits. Journal of the Mechanics and Physics of Solids, 1960, 8(2): 100-104. DOI: 10.1016/0022-5096(60)90013-2.

[18] Barenblatt G I. The mathematical theory of equilibrium cracks in brittle fracture. Advances in Applied Mechanics, 1962, 7(C): 55-129. DOI: 10.1016/S0065-2156(08)70121-2.

[19] ABAQUS. Analysis User's Manual (V6.6). Providence, RI: Dassault Systemes Simulia Corp, 2011.

[20] Alfano G, de Barros S, Champaney L, et al. Comparison between two cohesive-zone models for the analysis of interface debonding. European Congress on Computational Methods in Applied Sciences and Engineering (ECCOMAS). Neittaanmäki P, Rossi T, Majava K, et al (eds.), Owen R, Mikkola M (assoc. eds.) Jyväskylä, 2004.